AIAA JOURNAL
Vol. 39, No. 12, December 2001

Numerical Simulation of Jets in a Crossflow Using Different Turbulence Models

Mohammad Reza Keimasi* and Mohammad Taeibi-Rahni†
Sharif University of Technology, Tehran, 13145 Iran

Calculation of a three-dimensional turbulent flow of square jets injected perpendicularly into a crossflow is performed computationally. The jet-to-crossflow velocity ratios were selected to be 0.5, 1.0, and 1.5, and the jet Reynolds number was 4700 based on the jet diameter. We solved the Reynolds-averaged Navier–Stokes equations in the general form using the SIMPLE finite volume method over a nonuniform staggered grid. Our computational domain included the jet channel flows as well as the flow over a flat plate. For the turbulence modeling, the standard k–ε model with wall functions and the zonal $(k$–$\varepsilon)/(k$–$\omega)$ turbulence model (shear stress transport model) were used. The results of the two different turbulence models were compared with previous experimental data. It was noted that our results were much closer to the experimental data than those existing solutions of the same problem performed earlier.

Introduction

SEVERAL engineering applications exist in which jets enter a crossflow, such as in film cooling of gas turbine blades. To have greater jet engine efficiency, the turbine entrance temperature needs to be increased. On the other hand, structural limitations exist; thus, the turbine blades need to be somehow cooled. Because internal cooling of the blades is not always efficient, film cooling is usually used.

In this work, we computationally simulated a three-dimensional and incompressible flowfield of square jets injected perpendicularly into a crossflow over a flat plate. The jet-to-crossflow velocity ratios (blowing ratios) were selected to be 0.5, 1.0, and 1.5, and the jet Reynolds number was 4700. Also, the jet spacing-to-jet-width ratio in one row of holes was selected to be 3.0. We solved the Reynolds-averaged Navier–Stokes (RANS) equations (including energy equation) in the general form, using the SIMPLE finite volume method over a nonuniform staggered grid.

In this type of flow, the flowfield at the jet exit is three-dimensional and strongly depends on the jet-to-crossflow-velocity ratio R. Thus, it is much better to solve the flow in the jet channel together with the flow over the flat plate. In addition, we solved the same problem using a domain that included only the flow over the flat plate, whereas the experimental data at the jet exit were used as the related boundary conditions. The results of this case were then compared with other computational solutions, which included the jet channel flow.

For the turbulence modeling, the standard k–ε model with wall functions and zonal $(k$–$\varepsilon)/(k$–$\omega)$ turbulence model (shear stress transport model or SST) were used. The results of the two different turbulence models were compared with the experimental data of Ajersch et al.[1] Some of the zonal turbulence model results were found to be closer to the experimental data than those obtained by the standard k–ε model. Comparisons indicated that the ability of the SST model to predict our flowfield depends strongly on the velocity ratio as well as on the distance downstream of the jet. It is also important to note that our computational results were found to be much closer to the experimental data than those computational solutions obtained by Ajersch et al.[1]

Received 3 May 2000; revision received 26 February 2001; accepted for publication 6 March 2001.

*Graduate Student, School of Mechanical Engineering; kimasi@mehr.sharif.ac.ir.

†Assistant Professor, School of Mechanical Engineering; taeibi@sina.sharif.edu.

Literature Review

Many researchers have studied the flow of jets in a crossflow both computationally and experimentally. Ajersch et al.,[1] have studied the flow of a row of six square jets injected at 90 deg to a crossflow, both experimentally and computationally. Their jet-to-crossflow-velocity ratios (blowing ratios) examined were 0.5, 1.0, and 1.5, and their jet-spacing-to-jet-width ratio was 3.0. Also, their jet Reynolds number was 4700. They measured the mean velocities and the six Reynolds stresses using a three-component laser Doppler velocimeter operating in coincidence mode. On the other hand, their numerical simulation of the flow was performed using a multigrid, segmented, k–ε computational fluid dynamics code. Special near-wall treatment included a nonisotropic formulation for the effective viscosity, a low Reynolds-number model for k, and an algebraic model for the length scale. Their computational domain also included the jet channel. In their computational work, the velocities and the Reynolds stresses on the jet centerline downstream of the jet exit were not predicted well, probably due to the inadequate turbulence modeling, while the values off the centerline matched reasonably well with those of experiments.

Hassan et al.[2] numerically investigated the flowfield from a single row of compound-angle jets in a crossflow, using different zonal $(k$–$\varepsilon)/(k$–$\omega)$ turbulence models. Their results were compared with previous experimental data for jet-to-crossflow-velocity ratios of 0.5 and 1.5. These comparisons indicated that the ability of the zonal $(k$–$\varepsilon)/(k$–$\omega)$ turbulence models to predict the flowfield of a jet in a crossflow depends strongly on the velocity ratio as well as on the distance downstream from the injection holes.

Amer et al.[3] used different turbulence models to predict film cooling from two rows of holes inclined in the streamwise direction. Their models were the k–ω model and its modified version, as well as the standard k–ε model, together with its nonisotropic version. Comparison between the predicted results using these models and the previous experimental data indicated that the ability of a turbulence model to predict the experimental results depends strongly on the blowing ratio as well as on the distance downstream from the injection holes. Also, they investigated the effects of the various coolant velocities of the injection holes for the prediction of film cooling.

Kim and Benson[4,5] calculated a three-dimensional turbulent flow of a jet in a crossflow using a multiple-timescale turbulence model. Their computational domain included a circular jet channel such that the interaction between the jet and the crossflow could be simulated more accurately. Their work showed that the row of jets in a crossflow is characterized by a highly complex flowfield, including a horseshoe vortex and two helical vortices.

Garg and Gaugler[6] demonstrated the importance of the jet exit plane conditions on the downstream results. They performed

simulations for three different blade configurations using $\frac{1}{7}$th power-law and "tuned" polynomial jet exit profiles of velocity and temperature distributions. Their results indicated that the downstream heat transfer coefficient levels may differ by as much as 60%, depending on the jet exit profile used, highlighting the critical influence of the jet exit conditions on the results downstream of the jet.

Walters and Leylek[7] computationally solved a three-dimensional discrete jet in a crossflow using a systematic computational methodology. Their computational domain included the space above the flat plate, the jet channel, and the plenum region. Their solutions were obtained using a multiblock, unstructured/adaptive grid, fully explicit, time marching, Reynolds-averaged Navier–Stokes code (RAMPANT software package from Fluent). Their results demonstrated that the prescribed computational methodology consistently yields more accurate solutions for this class of problems than previous computational works.

Governing Equations

The computations were performed assuming a constant property flow. Under this assumption, the RANS equations are as follows:

$$\frac{\partial \bar{u}_j}{\partial x_j} = 0 \tag{1}$$

$$\frac{\partial}{\partial x_j}(\rho \bar{u}_i \bar{u}_j) = -\frac{\partial}{\partial x_i}\left(\bar{p} + \frac{2}{3}\rho k\right) + \frac{\partial}{\partial x_j}\left\{\mu_{\text{eff}}\left(\frac{\partial \bar{u}_i}{\partial x_j} + \frac{\partial \bar{u}_j}{\partial x_i}\right)\right\} \tag{2}$$

$$\frac{\partial}{\partial x_j}(\rho \bar{u}_j \bar{T}) = \frac{\partial}{\partial x_j}\left\{\left(\frac{\mu_l}{Pr_l} + \frac{\mu_t}{Pr_t}\right)\frac{\partial \bar{T}}{\partial x_j}\right\} \tag{3}$$

where ρ is density, k is turbulence kinetic energy, $\bar{p}$ is mean pressure, and μ_{eff} is effective viscosity ($\mu_{\text{eff}} = \mu_l + \mu_t$; μ_l and μ_t are the molecular and turbulent viscosities, respectively). Also, in Eq. (3) $\bar{T}$ is mean temperature and Pr_l and Pr_t are molecular and turbulent Prandtl numbers, respectively.

Jet-to-Crossflow Characteristics

Flowfield characteristics of jets in a crossflow are strongly dependent on the momentum ratio defined as

$$J = \frac{\rho_{\text{jet}} V_{\text{jet}}^2}{\rho_{\text{cf}} V_{\text{cf}}^2} \tag{4}$$

where the subscripts jet and cf correspond to jet and crossflow, respectively.[8] Here the mainstream and the jet fluids were considered both to be air and therefore J is replaced by velocity ratio, as

$$R = V_{\text{jet}}/V_{\text{cf}} \tag{5}$$

Three cases of R (0.5, 1.0, and 1.5) were considered in this study. For all of these cases, the jet velocity at the inlet of the channel (V_{jet}) was maintained at 5.5 m/s; therefore, the crossflow velocities used were 3.67, 5.5, and 11.0 m/s. The jet diameter D was 12.7 mm. Throughout this paper, references are made to the "diameter" of the jet. This terminology is rooted in the past study of jets, where round jets are customarily used. Thus, the term "diameter" is equivalent to the "jet width." Based on this length scale, a jet Reynolds number, defined as

$$Re_{\text{jet}} = \rho V_{\text{jet}} D/\mu \tag{6}$$

was obtained to be 4700, which was kept constant throughout this study.

Turbulence Models

The SST model developed by Menter[9,10] uses the k–ω model in the sublayer as well as in the logarithmic part of the boundary layer. In the wake region of the boundary layer, the k–ω model has to be abandoned in favor of the k–ε model. The reason for this switch is that the k–ω model has a very strong sensitivity to the freestream values of ω, but the k–ε model does not suffer from this deficiency. Unlike any other two-equation model, the k–ω model does not involve damping functions and, as will be shown later, allows simple Dirichlet boundary conditions to be specified.

The equations of the SST model are

$$\frac{\mathrm{D}\rho k}{\mathrm{D}t} = \tau_{ij}\frac{\partial \bar{u}_i}{\partial x_j} - \beta^*\rho\omega k + \frac{\partial}{\partial x_j}\left[(\mu + \sigma_k \mu_t)\frac{\partial k}{\partial x_j}\right] \tag{7}$$

$$\frac{\mathrm{D}\rho\omega}{\mathrm{D}t} = \frac{\gamma}{\upsilon_t}\tau_{ij}\frac{\partial \bar{u}_i}{\partial x_j} - \beta\rho\omega^2 + \frac{\partial}{\partial x_j}\left[(\mu + \sigma_\omega \mu_t)\frac{\partial \omega}{\partial x_j}\right] + 2\rho(1 - F_l)\sigma_{\omega 2}\frac{1}{\omega}\frac{\partial k}{\partial x_j}\frac{\partial \omega}{\partial x_j} \tag{8}$$

where ω is the specific dissipation rate ($\varepsilon/\beta^* k$), υ_t is the eddy kinematic viscosity, τ_{ij} are the Reynolds stresses, and the left-hand sides of the equations are the Lagrangian derivative ($\mathrm{D}/\mathrm{D}t = \partial/\partial t + u_i \partial/\partial x_i$). Also, the switching function F_l is such that it is unity near the surface and is zero away from it, resulting in the k–ω model in the near-wall region and the k–ε model in the remainder of the flowfield. The values of the constants σ_k, σ_ω, $\sigma_{\omega 2}$, β, β^*, γ, and relations defining the switching function F_l and υ_t are given by Menter.[9]

The standard k–ε model with wall functions was used in this work to compare the results with the SST model.

Computational Methodology

We developed a computer code to solve three-dimensional incompressible RANS equations (including the energy equation) using the SIMPLE finite volume method. This code uses a nonuniform staggered grid arrangement in which the velocity components are located on the control volume surfaces and the scalar quantities are located inside the control volumes. For the computation of fluxes, the power-law differencing scheme of Patankar[11] was used. With this differencing scheme, the resulting matrix of coefficients is diagonally dominant; therefore, the scheme is unconditionally stable. The discretized algebraic equations were solved using a line-by-line method with appropriate under-relaxation factors for faster convergence.[12]

Computational Domain

The schematic of the problem is shown in Fig. 1. Our computational domain included the jet channel and the space above the flat plate. A square jet was used in this study and jet diameter (jet width) was D, which was used as the length unit throughout this work. The origin of the coordinate system used was located at the center of the jet exit. The jet channel length was $5D$, and the crossflow region extended from $5D$ upstream of the center of the jet to $40D$ downstream. In the vertical direction, the domain extends $20D$ above the

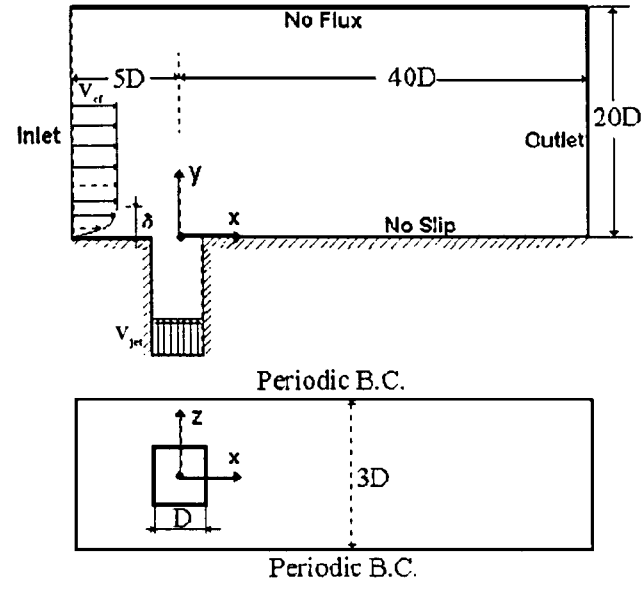

Fig. 1 Computational domain.

flat plate. The jets were injected into the crossflow perpendicularly, and the jet-spacing-to-jet-diameter ratio in one row of holes was taken to be 3.0.

Boundary Conditions

In this study, five types of boundary conditions—inlet, outlet, wall, no-flux, and periodic—were used. The inlet plane of the mainstream was located at a distance $5D$ upstream from the jet center. Here, the boundary layer thickness was set to $2D$ to match the experimental data. In the boundary layer, the $\frac{1}{7}$th power-law profile was used as the inlet boundary condition for $\bar{u}$-velocity component and a uniform velocity was imposed above $y = 2D$. The values of the turbulence kinetic energy, which was measured by Ajersch et al.,[1] were used as the inlet turbulence energy boundary condition. The value of this turbulence kinetic energy was approximately 2% of V_{cf} in the cases in which $R = 1.5$ and 1.0 and was about 1.2% of V_{cf} for $R = 0.5$. Also, the maximum turbulence kinetic energy in the boundary layer was on the order of 10% of V_{cf}. Turbulence was nonisotropic, with the magnitude of u'^2 being approximately twice that of either v'^2 or w'^2. When we used the k–ε model, the inlet turbulence dissipation rate was obtained from the approximate formula recommended by Versteeg and Malalasekera[12] as follows:

$$\varepsilon_{in} = C_{\mu}^{\frac{3}{4}} \left(k^{\frac{3}{2}} / L_m \right) \tag{9}$$

where C_μ is an experimental constant and is 0.09 and L_m is the Prandtl's mixing length scale. As suggested by Menter,[9] when we use the SST model the inlet value of ω is obtained using the following relation:

$$\omega_{in} = (1 \rightarrow 10)(V_{cf}/L) \tag{10}$$

where L is the approximate length of the computational domain. Note that uniform distribution of the vertical velocity and the turbulence kinetic energy were assumed at the channel inlet.

At the outlet boundary, special care was taken for the $\bar{u}$-velocity boundary condition. Calculation of $\bar{u}$ at the outlet plane ($i = \mathrm{NI}$, where NI is maximum number of grid points in the x direction) by assuming a zero gradient is such that

$$\bar{u}_{\mathrm{NI},J,k} = \bar{u}_{\mathrm{NI}-1,J,K} \tag{11}$$

Note that during the iteration cycles of the SIMPLE algorithm there is no guarantee that these velocities will conserve mass over the computational domain as a whole. To ensure that overall continuity is satisfied, the total mass flux going out of the domain $\dot{M}_{out}$ is first computed, using the extrapolated outlet velocities [Eq. (11)]. To make the outgoing mass flux equal to the incoming one ($\dot{M}_{in}$), all outlet velocity components are multiplied by the ratio $\dot{M}_{in}/\dot{M}_{out}$. Thus, the outlet plane velocities with the continuity correction are given as

$$\bar{u}_{\mathrm{NI},J,k} = \bar{u}_{\mathrm{NI}-1,J,K}(\dot{M}_{in}/\dot{M}_{out}) \tag{12}$$

For other dependent variables, their extrapolated values were used at the outlet boundary.

At the top impermeable boundary, a free-slip condition was imposed, whereas the bottom wall was assumed adiabatic and a no-slip condition was applied therein. The same boundary conditions were used for the jet channel walls. Also, the standard wall functions were used for near the walls when the standard k–ε model was implemented. For the SST model, the turbulence kinetic energy was set to zero at the walls and ω was obtained by the following relation suggested by Menter[9]:

$$\omega = 60\upsilon / \beta_1 (\Delta y_1)^2 \qquad \text{at} \qquad y = 0 \tag{13}$$

where Δy_1 is the distance to the next point away from the wall, υ is the molecular kinematic viscosity, and β_1 is a constant. Finally, the periodic boundary condition was imposed in the spanwise direction.

Grid Resolution Study

We solved the film cooling problem with five different grids to obtain a grid-independent solution. The grids were nonuniform and were clustered near the wall in the y direction as well as at the jet exit in the x and z directions. The number of grid points in each direction for those five grids is given in Table 1.

We chose a sensitive parameter (turbulence kinetic energy) to compare the results obtained using different grids. The profile of the turbulence kinetic energy for $z/D = 0$ at $x/D = 5$ is shown in Fig. 2. The results related to case 1 are shown to have significant discrepancies with other cases, whereas the results of the fourth and fifth cases are reasonably close. Thus, the grid of case 4 was used in our study. Also, a $7 \times 30 \times 7$ grid was used in the jet channel. The grid at the x–y plane is shown in Fig. 3.

Discussion of Results

The computed results of the standard k–ε and the SST turbulence models were compared with the experimental results of Ajersch

Table 1 Number of grid points for five different grids used

Case	NI	NJ	NK	N_{total}
1	60	40	15	36,000
2	78	50	17	66,500
3	148	70	17	176,000
4	188	83	17	265,000
5	230	100	21	500,000

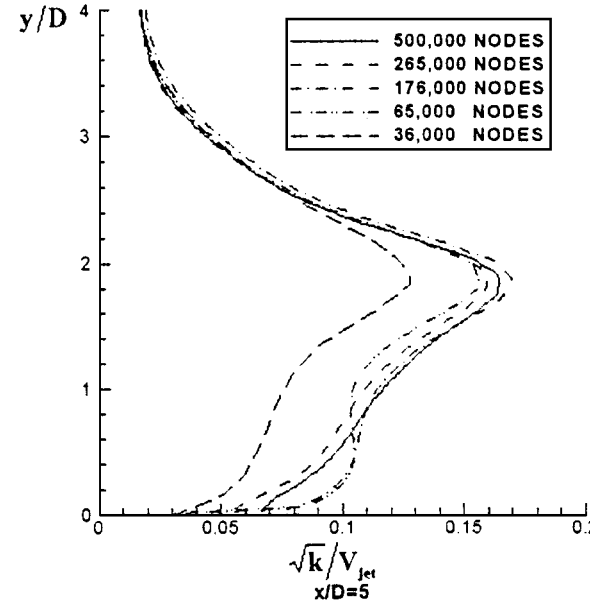

Fig. 2 Comparison of turbulence kinetic energy at jet center plane ($z/D = 0$) obtained by different grids.

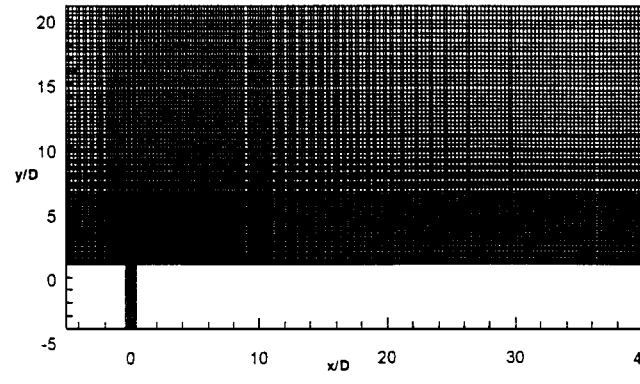

Fig. 3 Nonuniform grid at x–y plane (265,000 nodes).

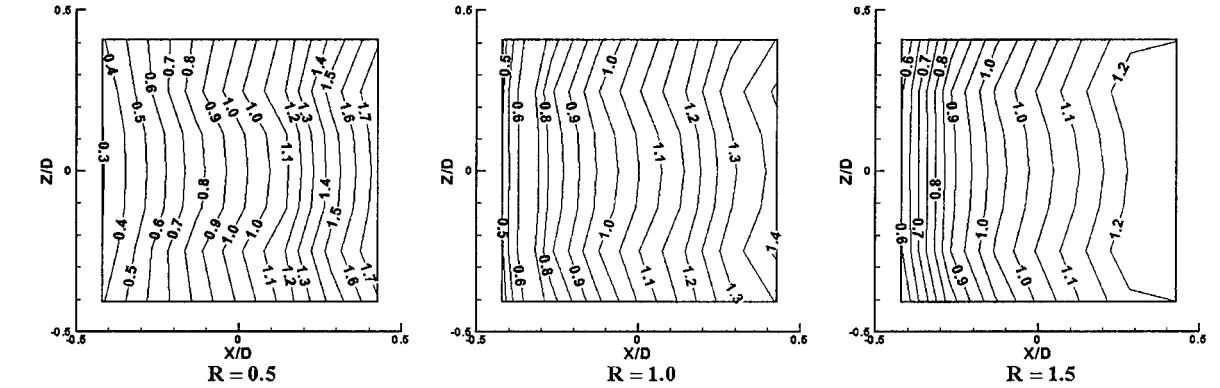

a) Computational

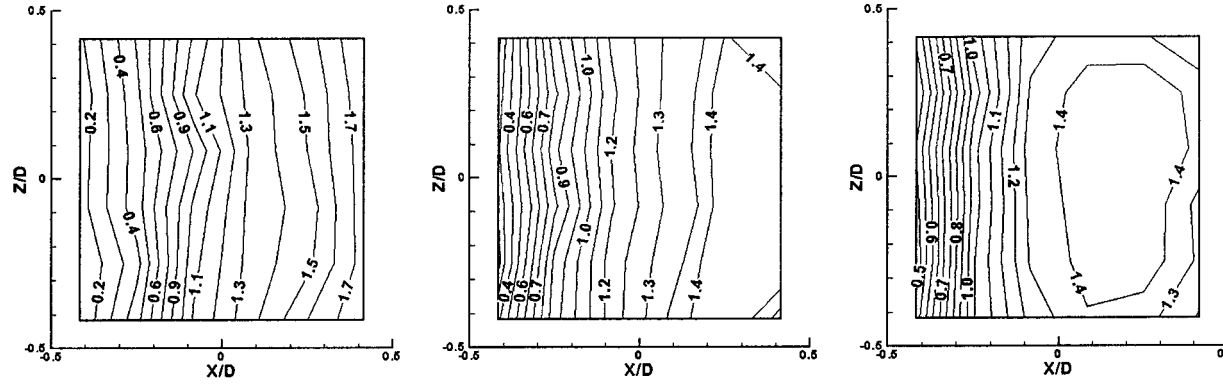

b) Experimental[1]

Fig. 4 Distribution of vertical velocity $\bar{v}/V_{jet}$ at the jet exit ($y/D = 0$) for different velocity ratios.

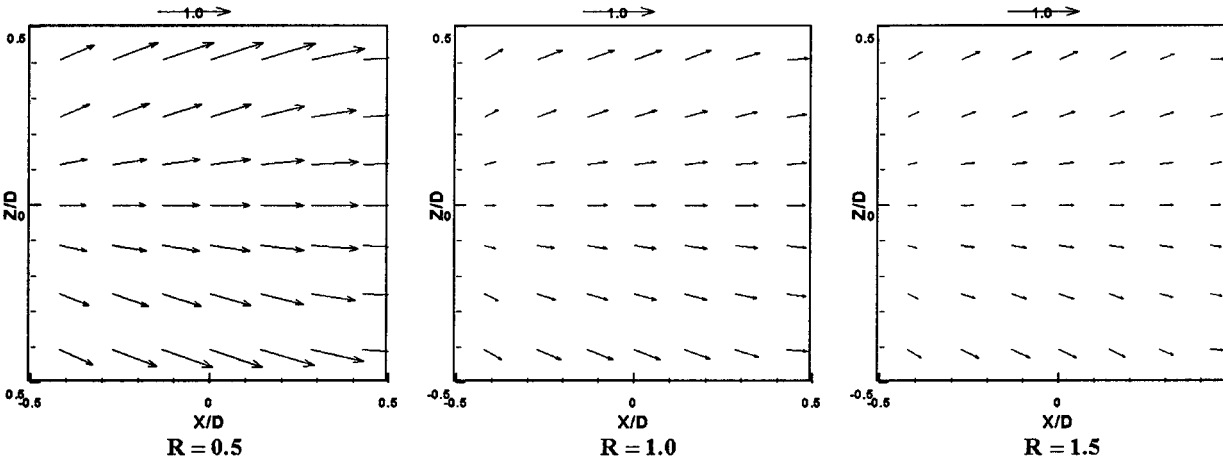

a) Computational

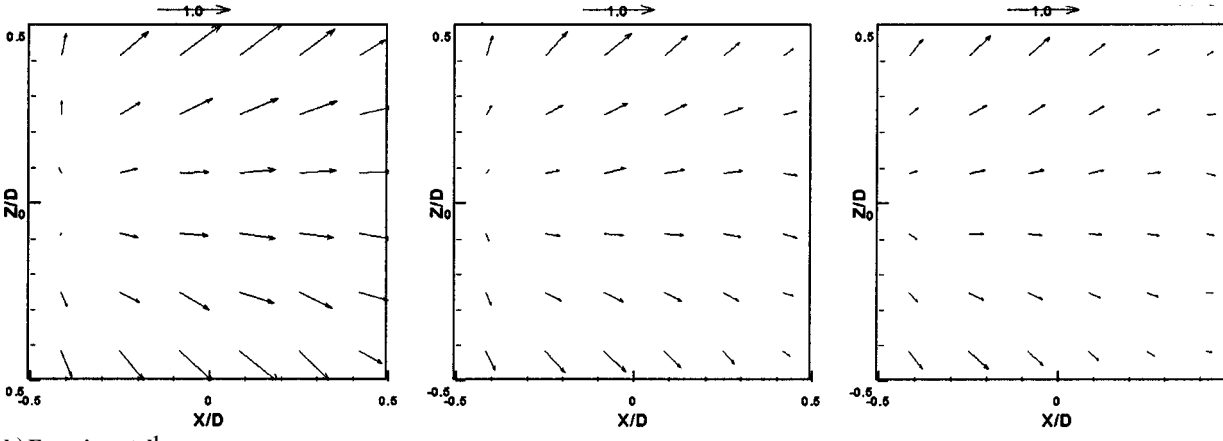

b) Experimental[1]

Fig. 5 Velocity vectors $\bar{V}/V_{jet}$ at the jet exit plane for different velocity ratios.

et al.[1] for three different velocity ratios, 0.5, 1.0, and 1.5. The results are divided into the ones related to the jet exit conditions, mean velocity fields, mean velocity profiles, and turbulence intensities (see also Keimasi[13] for more details).

Jet Exit Conditions

Both the measured data and our computational solution show that the jet and the crossflow interact strongly. Also, the flowfield at the jet exit is strongly dependent on the jet-to-crossflow-velocity ratio. Therefore, the velocity boundary condition used in a number of previous numerical calculations (e.g., those of Refs. 3 and 6) are not truly valid approximations for the fluid flow at the jet exit.

The nondimensional vertical velocity contours at the jet exit for three different velocity ratios (0.5, 1.0, and 1.5) are shown in Fig. 4, where Fig. 4a represents our computational results and Fig. 4b shows Ajersch's[1] experimental data. Qualitative comparisons of Figs. 4a and 4b demonstrate that the vertical velocity values obtained by our computational solution have reasonable agreement with those obtained experimentally. Note also that the relatively stronger jet ($R = 1.5$) is least affected by the crossflow, whereas the weak jet ($R = 0.5$) has been deflected by the crossflow significantly. Also, the value of $\bar{v}/V_{\text{jet}}$ for $R = 0.5$ obtained by computational solution varies from 0.3 upstream to 1.7 downstream, whereas for $R = 1.5$, $\bar{v}/V_{\text{jet}}$ varies from 0.6 to 1.2. For all velocity ratios, the variation of $\bar{v}/V_{\text{jet}}$ upstream is higher than that downstream. However, the profile becomes more uniform for high velocity ratios.

The nondimensional velocity vectors in the jet exit plane, obtained by our computational simulations, are shown in Fig. 5a, whereas Fig. 5b shows the ones obtained experimentally. These computational and experimental results show reasonable agreements. The streamwise deflection of the jet in all cases is shown very clearly and, as expected, it is the strongest for the case $R = 0.5$. Transverse deflection also exists, and its value is increased with distance away from the jet centerline ($z/D = 0$). Both computational and experimental results show symmetry about this centerline in all three cases.

A typical computed turbulence kinetic energy at the jet exit plane for the velocity ratio of $R = 1.5$ is shown in Fig. 6a, whereas Fig. 6b demonstrates the corresponding experimental data. In contrast to the velocity field, the distribution of the turbulence kinetic energy at the jet exit obtained computationally in this work does not match well with the experimental data. This is also the case for other velocity ratios (not shown here). This difference is mainly due to the jet inlet boundary condition, where uniform turbulence kinetic energy and vertical velocity were assumed as our boundary conditions. In the experimental setup used by Ajersch et al.,[1] the quiescent fluid in the plenum accelerates around the sharp edges of the inlet into the jet channel, so that the turbulence kinetic energy becomes nonuniform. This emphasizes the importance of solving flow in the plenum together with the rest of the flowfield.

Because the distribution of the turbulence kinetic energy at the jet exit obtained computationally is different from the experimental data, we also solved the problem using the existing experimental data as the boundary condition at the jet exit. Obviously, in this case, our computational domain did not include the jet channel. The results of this case were compared with the case in which the domain included the jet channel and also with the experimental results. (The results of this case will be discussed later in this paper.)

Mean Velocity Field

The most important feature of the jet in a crossflow is the interaction between the two crossing flows. Figure 7 shows the nondimensional velocity vectors in the jet center plane ($z/D = 0$) for the velocity ratio of $R = 0.5$. Note that the trajectory of the jet is deflected into the streamwise direction, whereas the crossflow is altered as if it is blocked by a rigid obstacle. However, because of the jet entrainment effects and the motion of the jet (compared to a fixed body), the jet in the crossflow results are somewhat different from flow over a rigid obstacle. It is also shown that the downstream region of the flowfield can be divided into three regions: wake region, jet region, and freestream region. Also, a reverse-flow region appears downstream of the jet exit, which indicates the existence of a three-dimensional separation. According to Andreopoulos and

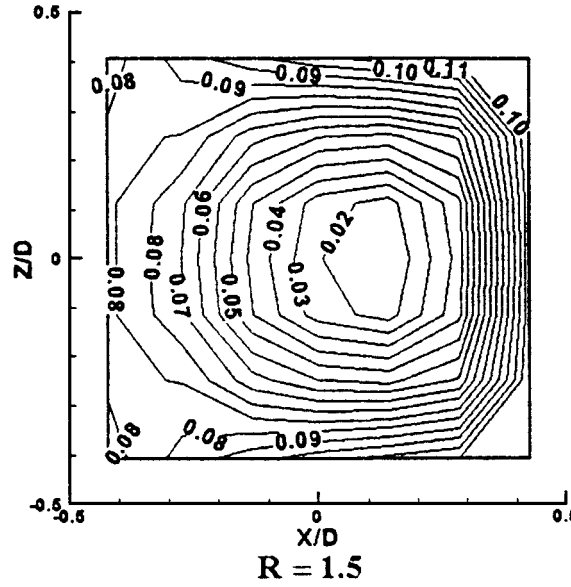

a) Computational

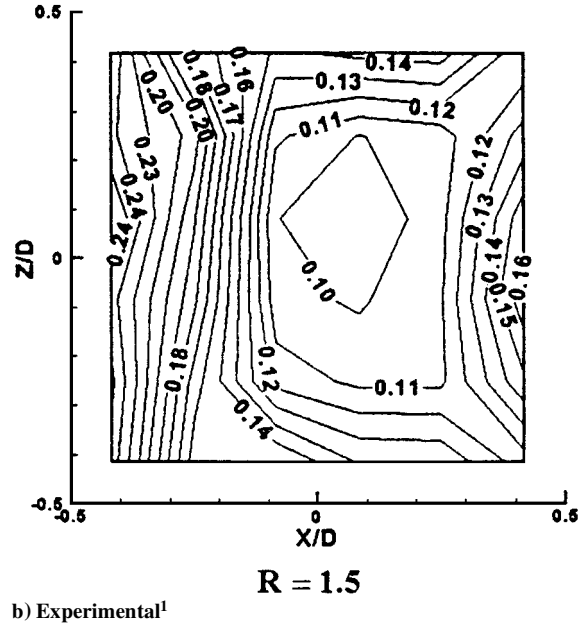

b) Experimental[1]

Fig. 6 Distribution of turbulence kinetic energy $\sqrt{k}/V_{\text{jet}}$ at the jet exit for the velocity ratio of 1.5.

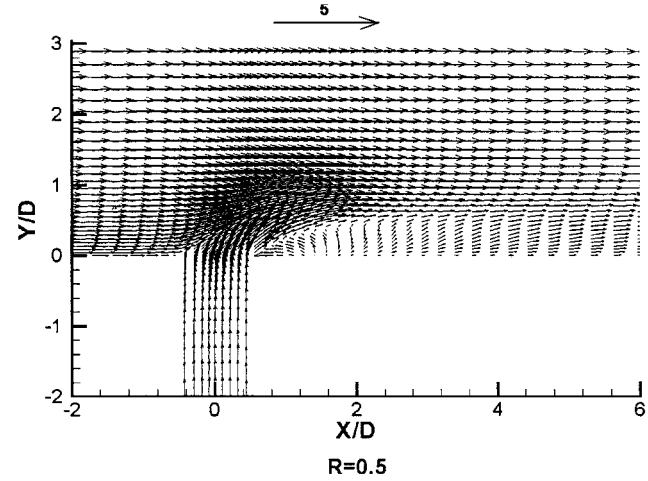

Fig. 7 Velocity vectors $\bar{V}/V_{\text{jet}}$ at jet center plane ($z/D = 0$) for the velocity ratio of 0.5.

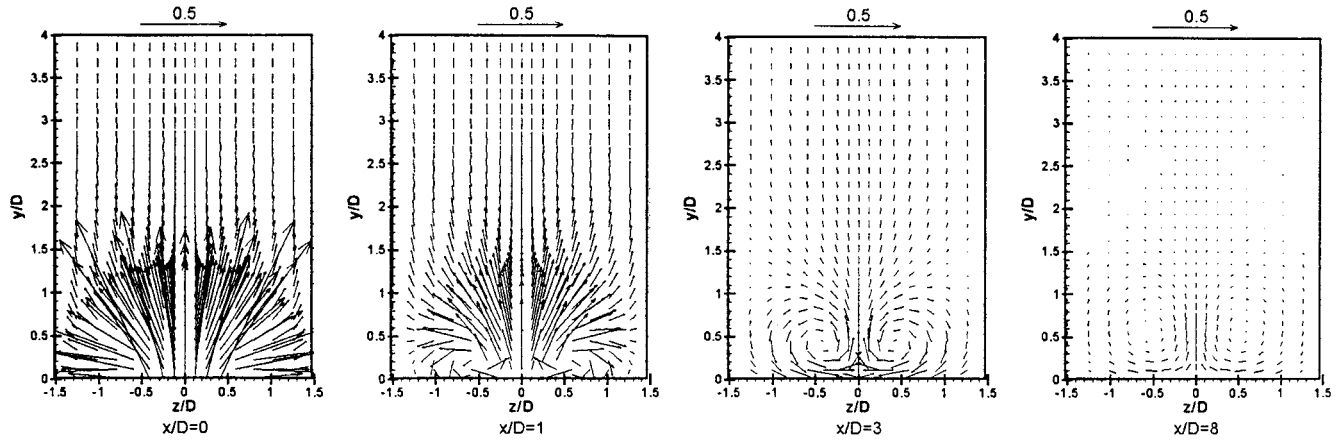

Fig. 8 Velocity vectors at different spanwise planes for the velocity ratio of 0.5.

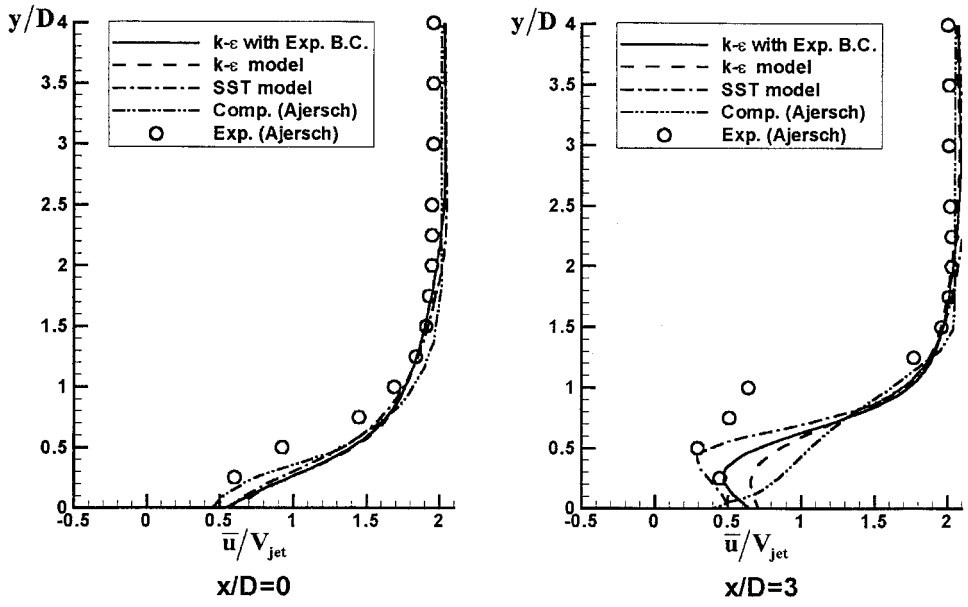

Fig. 9 Comparison of streamwise velocity at jet center plane ($z/D = 0$) for $R = 0.5$.

Rodi,[14] in this type of flow, a streamline follows a spiral path as it approaches the jet center plane. It is also shown that the crossflow is decelerated rapidly by the jet; thus, the pressure is increased in the upstream region of the jet.

The three-dimensional nature of the flowfield is illustrated by the velocity fields of Fig. 8, which shows the nondimensional velocity vector fields at different spanwise planes ($x/D = 0$, 1, 3, and 8) for $R = 0.5$. At $x/D = 0$, the vertical velocity component has a relatively large value. However, in the region where z/D is larger than 0.5, the transverse component of the velocity is dominant in the near-wall region. The flow parallel to the wall is due to the injection of the jet, which results in pushing the crossflow fluid out in the transverse direction. Also, it is observed that a counter-rotating vortex pair (CRVP) starts to appear at $x/D = 1$ and its strength decreases downstream. Note that the strength of the CRVP and its distance from the flat plate increase with velocity ratio (not shown here). Also, the pressure drop in the wake region induces an inward motion, transporting the fluid from the crossflow toward the jet center plane. Thus, at $x/D = 1$, the somewhat irregular motion near the wall is due to the inward motion, which is balanced by the outward flow generated by the jet on either side of the jet exit.

Mean Velocity Profiles

Our computed mean velocity profiles using the k–ε and SST turbulence models are compared with each other, as well as with the computational and experimental data of Ajersch et al.[1] As mentioned earlier, to show the importance of the jet exit conditions, we have computationally solved the problem using experimental data as our jet exit boundary condition and compared the related results to the cases that included the jet channel flow.

The profiles of the streamwise velocity at the jet center-plane for different streamwise locations ($x/D = 0$ and 3) and $R = 0.5$ are shown in Fig. 9, and Fig. 10 shows the same profiles for $R = 1.5$. At $x/D = 0$, for the two velocity ratios, the results of the SST and the k–ε turbulence models are the same and show good agreement with Ajersch's experimental and computational data.[1] At locations farther downstream (e.g., $x/D = 3.0$) the difference between the k–ε and SST models is enhanced, which supports the previous findings (e.g., Hassan et al.[2] and Amer et al.[3]). Also, note that at $x/D = 3$, the streamwise velocity in the jet wake region obtained computationally by Ajersch[1] is overpredicted, especially for the case $R = 1.5$, whereas the reduction of the velocity in this region is captured well in all our computational solutions.

Figures 11 and 12 show the vertical velocity profiles at $z/D = -1$ (at $x/D = 0$ and 3) for $R = 0.5$ and 1.5, respectively. These figures demonstrate the downflow, which exists on the outer edge of the CRVP. The results of different turbulence models used in this study show negligible differences for case $R = 0.5$. Also, note that the magnitude of the downflow is underpredicted in our computational simulation for case $R = 0.5$ and it is captured better for $R = 1.5$. In the near field of the jet, the results for case $R = 1.5$ have obvious differences compared to the experimental data. For the case $R = 1.5$, the results show better agreement with the measurements when we use experimental data as the boundary conditions at the jet exit plane. This case is shown as "k–ε with Exp. B.C." in the figures.

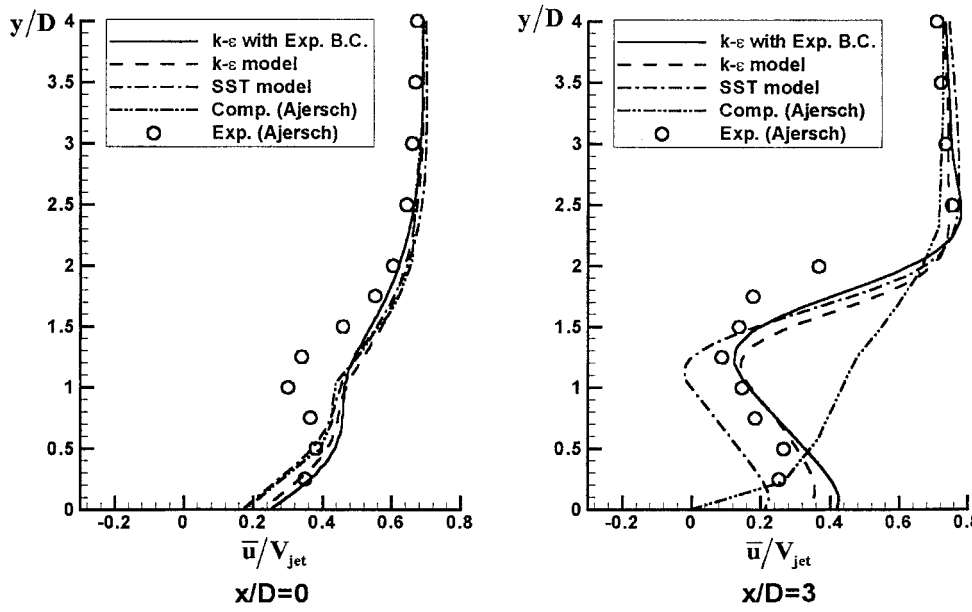

Fig. 10 Comparison of streamwise velocity at jet center plane ($z/D = 0$) for $R = 1.5$.

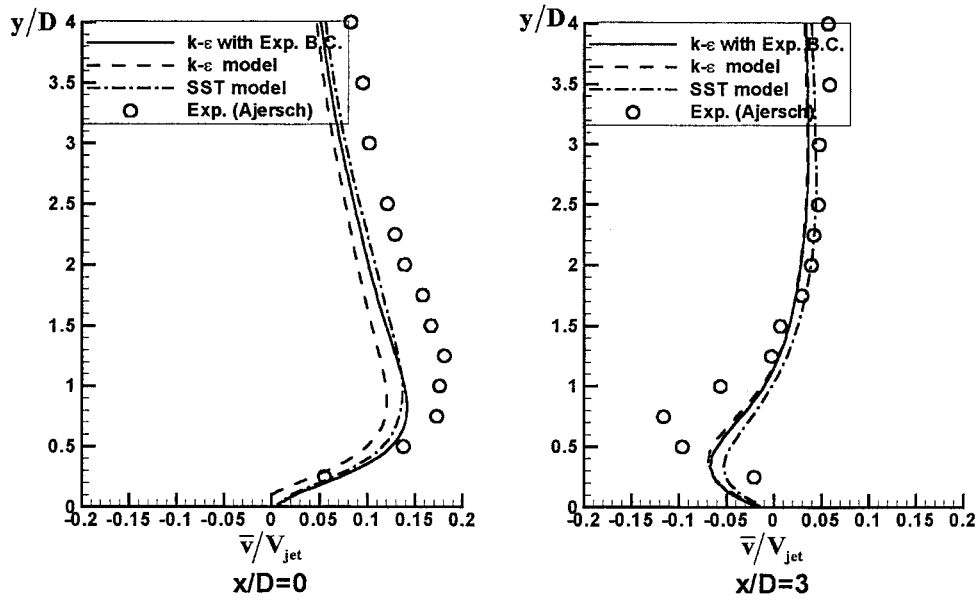

Fig. 11 Comparison of vertical velocity at $z/D = -1.0$ for $R = 0.5$.

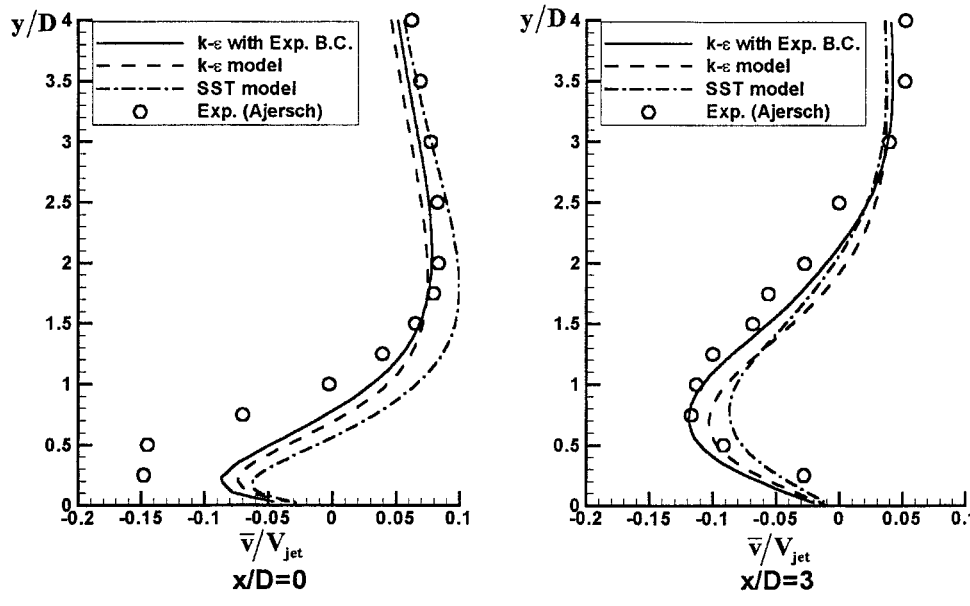

Fig. 12 Comparison of vertical velocity at $z/D = -1.0$ for $R = 1.5$.

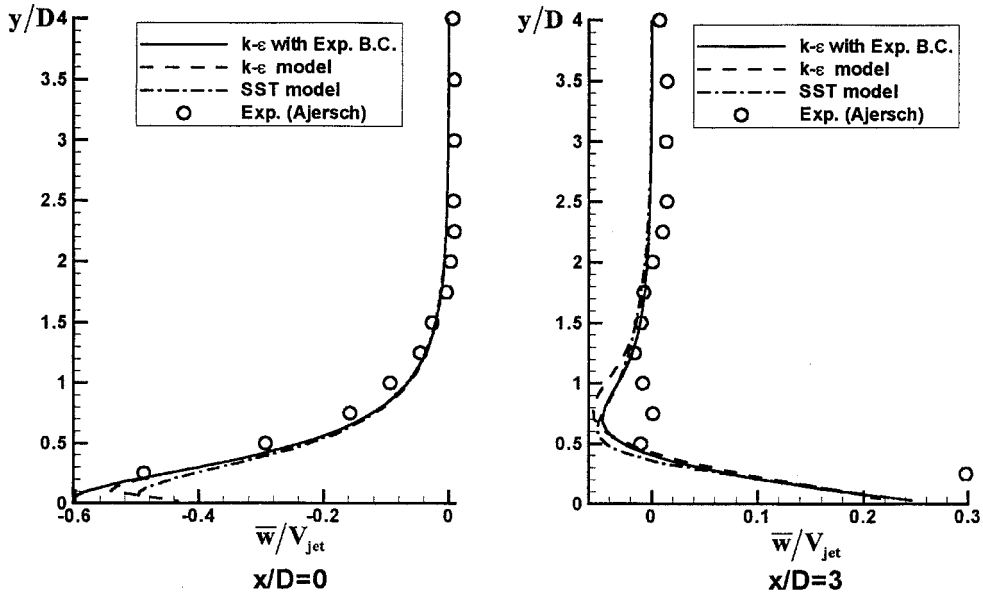

Fig. 13 Comparison of transverse component of velocity at $z/D = -0.5$ for $R = 0.5$.

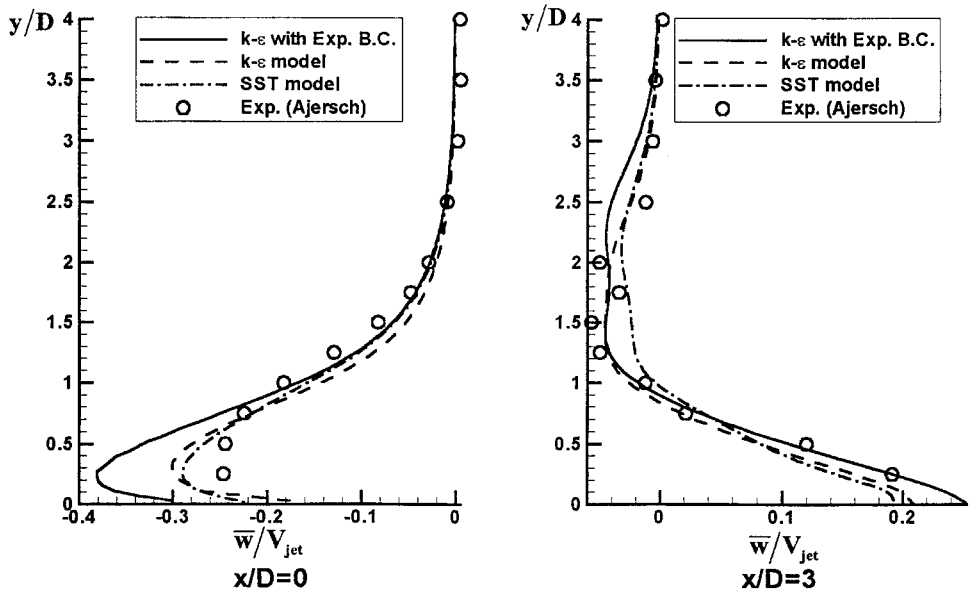

Fig. 14 Comparison of transverse component of velocity at $z/D = -0.5$ for $R = 1.5$.

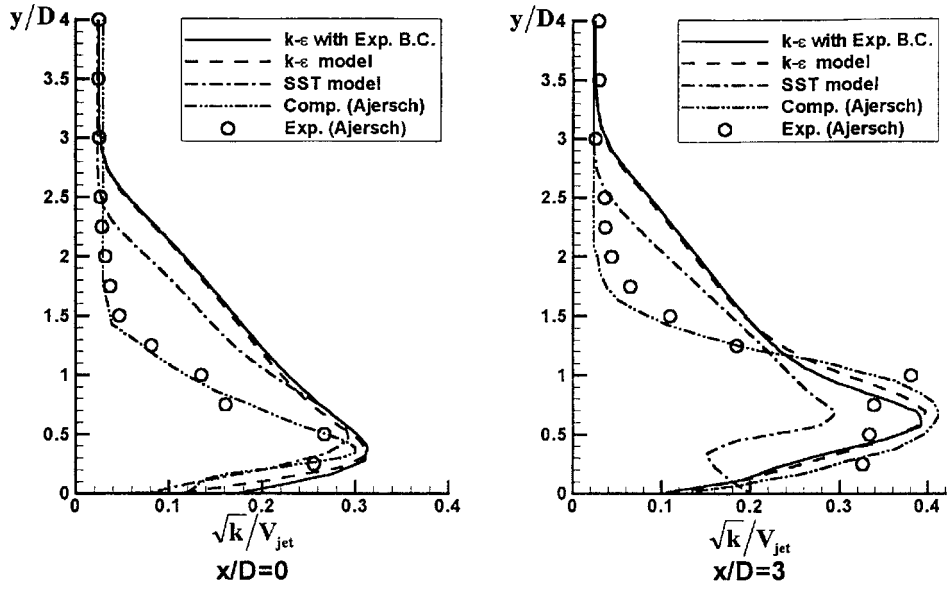

Fig. 15 Comparison of turbulence kinetic energy at jet center plane for $R = 0.5$.

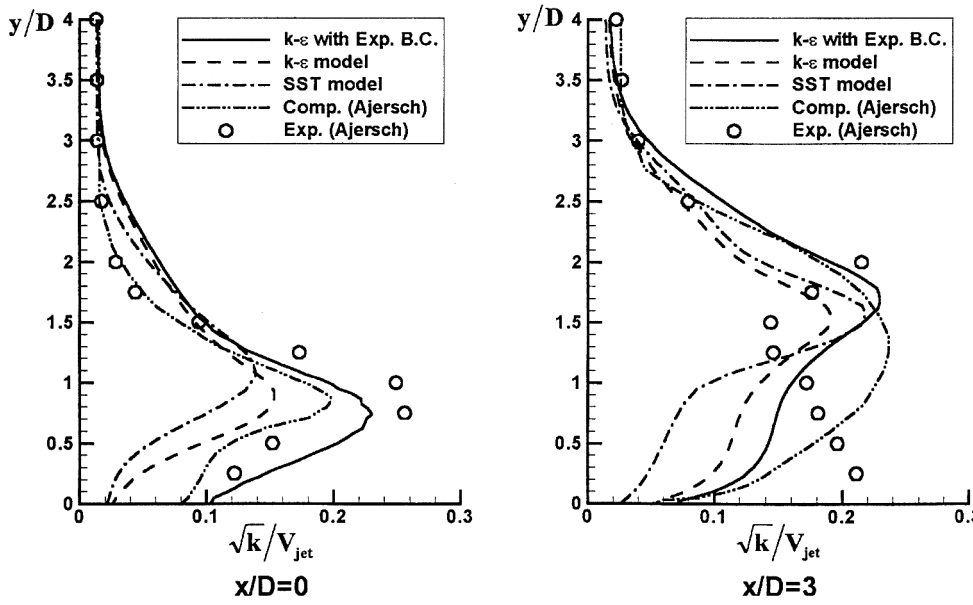

Fig. 16 Comparison of turbulence kinetic energy at jet center plane for $R = 1.5$.

Figures 13 and 14 show the transverse component of the velocity at $z/D = -0.5$ (at $x/D = 0$ and 3) for $R = 0.5$ and 1.5, respectively. Here, agreement with experimental data is better, whereas the results of the SST and the k–ε turbulence models show negligible differences.

Turbulence Kinetic Energy

The profiles of the turbulence kinetic energy ($\sqrt{k}/V_{\text{jet}}$) in the jet center plane at different streamwise locations for $R = 0.5$ and 1.5 are shown in Figs. 15 and 16, respectively. For $R = 0.5$ (Fig. 15), our computational results do not match well with the experimental data. Note that the use of the experimental data as our boundary condition at the jet exit did not affect these results considerably. For $R = 1.5$ (Fig. 16), our results are somewhat better in comparison with the case $R = 0.5$. As discussed earlier, the distribution of the turbulence kinetic energy at the jet exit obtained by our computational simulation did not match well with the experimental data. Thus, at $x/D = 0$, the peak of the turbulence kinetic energy is captured better when we used experimental data as our boundary condition at the jet exit.

For large x/D, the local minimum of $\sqrt{k}/V_{\text{jet}}$, which turned out to be located in the wake region, is not captured well in our computational solutions or in Ajersch's computational work.[1] This difficulty consistently exists when the SST model, the k–ε model, or the k–ε model with the experimental data at the jet exit are used. In addition, the peak of the turbulence kinetic energy near the wall was not captured well in any of these solutions. This is because the nature of this quantity is such that it grows very sharply in a very small distance away from the wall (in the sublayer) and is therefore very difficult to capture computationally.

Conclusions

In this study, a three-dimensional flowfield of normal jets in a crossflow was computationally simulated. For the turbulence modeling, the SST [zonal $(k$–$\varepsilon)/(k$–$\omega)$ turbulence model] and the standard k–ε models were used. The results of this computational simulation were compared with previous existing computational and experimental results for three different velocity ratios ($R = 0.5$, 1.0, and 1.5).

The computational results related to the mean velocity profiles agreed well with the experimental data, whereas there were some differences in the turbulence kinetic energy. The experimental data of Ajersch et al.[1] have shown a highly nonisotropic turbulence, particularly at high velocity ratios. Thus, one of the error sources in the simulation of this complex flowfield is the anisotropy, which is not considered by the turbulence models used here. In comparison with Ajersch's computational solution,[1] our computational results showed better agreements with experimental data (especially the mean streamwise velocity profiles).

Note that, in this study, the flow in the jet channel was also solved with the main flow. It was found that vertical velocity at the jet exit plane was nonuniform, especially for the low velocity ratio (0.5). The distribution of the velocity vector field at the jet exit agreed reasonably well with the experimental results, whereas the results for the turbulence kinetic energy did not agree as well there.

Besides the cases where we solved the jet channel flow together with the main flow, we also performed our computational simulation using the experimental data as our boundary condition at the jet exit plane. Overall, this boundary condition gave better results, especially for the turbulence kinetic energy. As noted by others (e.g., Ajersch et al.[1]) a computational domain that also includes the plenum is necessary to predict the flow at the jet exit plane more accurately.

Also, as noted by others,[1,14] a reversed flow region appeared downstream of the jet exit for the three velocity ratios used in this study. The size of this region is the smallest for the case $R = 0.5$, in which the reversed flow region is much closer to the wall due to the stronger deflection of the jet. Also, the CRVP is observed for all velocity ratios in this simulation. Of course, the strength of the CRVP decreases with downstream positions. It was also found that, for the case $R = 0.5$, the CRVP disappears at about $x/D = 8$.

Acknowledgments

This work was supported by the research funds of Sharif University of Technology, under supervision of Mohammad Kermanshah. The support of the Department of Mechanical Engineering at that university is also acknowledged.

References

[1] Ajersch, P., Zhou, J. M., Ketler, S., Salcudean, M., and Gartshore, I. S., "Multiple Jets in a Crossflow: Detailed Measurements and Numerical Simulations," International Gas Turbine and Aeroengine Congress and Exposition, ASME Paper 95-GT-9, Houston, TX, June 1995, pp. 1–16.

[2] Hassan, I., Findlay, M., Salcudean, M., and Gartshore, I., "Prediction of Film Cooling with Compound-Angle Injection Using Different Turbulence Models," 6th Annual Conf. of the Computational Fluid Dynamics Society of Canada, Quebec, QC, Canada, June 1998, pp. 1–6.

[3] Amer, A. A., Jubran, B. A., and Hamdan, M. A., "Comparison of Different Two-Equation Turbulence Models for Prediction of Film Cooling from Two Rows of Holes," *Numerical Heat Transfer*, Pt. A, Vol. 21, 1992, pp. 143–162.

[4] Kim, S. W., and Benson, T. J., "Calculation of a Circular Jet in Crossflow with a Multiple-Time-Scale Turbulence Model," *International Journal of Heat and Mass Transfer*, Vol. 35, No. 10, 1992, pp. 2357–2365.

[5]Kim, S. W., and Benson, T. J., "Fluid Flow of a Row of Jets in Crossflow—A Numerical Study," *AIAA Journal*, Vol. 31, No. 5, 1993, pp. 806–811.

[6]Garg, V. K., and Gaugler, R. E., "Effect of Velocity and Temperature Distribution at the Hole Exit on Film Cooling of Turbine Blades," International Gas Turbine and Aeroengine Congress and Exposition, ASME Paper 95-GT-2, Houston, TX, June 1995, pp. 1–12.

[7]Walters, D. K., and Leylek, J. H., "A Systematic Computational Methodology Applied to a Three-Dimensional Film Cooling Flow Field," *Journal of Turbomachinery*, Vol. 119, 1997, pp.777–785.

[8]Holdeman, J. D., and Walker, R. E., "Mixing of a Row of Jets with a Confined Crossflow," *AIAA Journal*, Vol. 15, No. 2, 1977, pp. 243–249.

[9]Menter, F. R., "Two-Equation Eddy-Viscosity Turbulence Models for Engineering Applications," *AIAA Journal*, Vol. 32, No. 8, 1994, pp. 1598–1605.

[10]Menter, F. R., "Performance of Popular Turbulence Models for Attached and Separated Adverse Pressure Gradient Flows," *AIAA Journal*, Vol. 30, No. 8, 1992, pp. 2066–2072.

[11]Patankar, S. V., *Numerical Heat Transfer and Fluid Flow*, Hemisphere, New York, 1980, Chap. 5.

[12]Versteeg, H. K., and Malalasekera, W., *An Introduction to Computational Fluid Dynamics—The Finite Volume Method*, Logman Malaysia, reprinted 1996, Chaps. 5–7.

[13]Keimasi, M. R., "Numerical Simulation of Film Cooling in a Turbulent Flow," M.Sc. Thesis, Dept. of Mechanical Engineering, Sharif Univ. of Technology, Tehran, Iran, Oct. 1999.

[14]Andreopoulos, J., and Rodi, W., "Experimental Investigation of Jets in a Cross Flow," *Journal of Fluid Mechanics*, Vol. 138, 1984, pp. 93–127.

R. M. C. So
Associate Editor